

**First-in-Human Application of Terbium-161: A Feasibility Study Using <sup>161</sup>Tb-DOTATOC**

Richard P. Baum<sup>1†\*</sup>, Aviral Singh<sup>1,2†</sup>, Harshad R. Kulkarni<sup>1</sup>, Peter Bernhardt<sup>3,4</sup>, Tobias Rydén<sup>3,4</sup>,  
Christiane Schuchardt<sup>1</sup>, Nadezda Gracheva<sup>5</sup>, Pascal V. Grundler<sup>5</sup>, Ulli Köster<sup>6</sup>, Dirk Müller<sup>7</sup>, Michael  
Pröhl<sup>7</sup>, Jan Rijn Zeevaart<sup>8</sup>, Roger Schibli<sup>5,9</sup>, Nicholas P. van der Meulen<sup>5,10</sup>, Cristina Müller<sup>5\*</sup>

<sup>1</sup> *Theranostics Center for Molecular Radiotherapy and Precision Oncology, ENETS Center of Excellence, Zentralklinik Bad Berka, Bad Berka, Germany*

<sup>2</sup> *GROW - School for Oncology and Developmental Biology, Maastricht University Medical Center, Maastricht, Netherlands*

<sup>3</sup> *Department of Radiation Physics, The Sahlgrenska Academy, University of Gothenburg, Sweden*

<sup>4</sup> *Department of Medical Physics and Medical Bioengineering, Sahlgrenska University Hospital, Gothenburg, Sweden*

<sup>5</sup> *Center for Radiopharmaceutical Sciences ETH-PSI-USZ, Paul Scherrer Institute, Villigen-PSI, Switzerland;*

<sup>6</sup> *Institut Laue Langevin, Grenoble, France*

<sup>7</sup> *Department of Radiopharmacy, Zentralklinik Bad Berka, Germany*

<sup>8</sup> *Radiochemistry, South African Nuclear Energy Corporation (Necsa), Pelindaba, South Africa*

<sup>9</sup> *Department of Chemistry and Applied Biosciences, ETH Zurich, Zurich, Switzerland*

<sup>10</sup> *Laboratory of Radiochemistry, Paul Scherrer Institute, Villigen-PSI, Switzerland*

† contributed equally

**\*Corresponding authors:**

PD Dr. Cristina Müller, PhD (ORCID: 0000-0001-9357-9688)

Center for Radiopharmaceutical Sciences ETH-PSI-USZ

Paul Scherrer Institute

5232 Villigen-PSI

Switzerland

e-mail: [cristina.mueller@psi.ch](mailto:cristina.mueller@psi.ch)

phone: +41-56-310 44 54

fax: +41-56-310 28 49

Prof. Dr. Richard P. Baum, MD (ORCID: 0000-0003-1723-0075)

CURANOSTICUM Wiesbaden-FrankfurtP

DKD Helios Klinik

Aukammallee 33

65191 Wiesbaden

Germany

e-mail: [baum@curanosticum.de](mailto:baum@curanosticum.de)

phone: +49 611 95 00 68 15

fax: +49 611 57 75 87

**Running title:** First-in-Man Application of Terbium-161

## ABSTRACT

$^{161}\text{Tb}$  has similar decay properties as  $^{177}\text{Lu}$  but, additionally, emits a substantial number of conversion and Auger electrons. The aim of this study was to apply  $^{161}\text{Tb}$  in a clinical setting and to investigate the feasibility to visualize the physiological and tumor biodistribution of  $^{161}\text{Tb}$ -DOTATOC. **Methods:**  $^{161}\text{Tb}$  was shipped from Paul Scherrer Institute, Switzerland, to Zentralklinik Bad Berka, Germany, where it was used for the radiolabeling of DOTATOC. In two separate studies, 596 MBq and 1300 MBq  $^{161}\text{Tb}$ -DOTATOC were administered to a 35-year-old male patient with metastatic, well differentiated, non-functional malignant paraganglioma and a 70-year-old male patient with a metastatic, functional neuroendocrine neoplasm of the pancreatic tail, respectively. Whole-body planar  $\gamma$ -scintigraphies were acquired over a period of several days for dosimetry calculations. SPECT/CT images were reconstructed, using a recently-established protocol and visually analyzed. Patients were checked for adverse events after application of  $^{161}\text{Tb}$ -DOTATOC. **Results:** The radiolabeling of DOTATOC with  $^{161}\text{Tb}$  was readily achieved with high radiochemical purity suitable for patient application. Planar images and dosimetry provided the expected time-dependent biodistribution of  $^{161}\text{Tb}$ -DOTATOC in liver, kidneys, spleen and urinary bladder. SPECT/CT images were of high quality and visualized even small metastases in the liver and bones. Application of  $^{161}\text{Tb}$ -DOTATOC was well tolerated and no related adverse events were reported. **Conclusion:** This study demonstrated the feasibility to image even small metastases after injection of relatively low activities of  $^{161}\text{Tb}$ -DOTATOC using  $\gamma$ -scintigraphy and SPECT. Based on this essential first step to translate  $^{161}\text{Tb}$  to clinics, further efforts will be directed towards the application of  $^{161}\text{Tb}$  for therapeutic purposes.

**Keywords:**  $^{161}\text{Tb}$ , SPECT/CT imaging, DOTATOC, Auger electrons, first-in-human

## INTRODUCTION

Terbium comprises four medically interesting radioisotopes ( $^{149}\text{Tb}$ ,  $^{152}\text{Tb}$ ,  $^{155}\text{Tb}$ ,  $^{161}\text{Tb}$ ), potentially useful for various applications in nuclear medicine while using chemically identical radiopharmaceuticals (1). Several years ago, the production and a preliminary preclinical application of all four Tb radioisotopes was demonstrated at Paul Scherrer Institute in Switzerland (2). Since then, additional studies have been performed with the aim to improve the production methods (3) and to investigate the potential of these radioisotopes for nuclear imaging ( $^{152}\text{Tb}$ ,  $^{155}\text{Tb}$ ) (4,5) and targeted radionuclide therapy ( $^{149}\text{Tb}$ ,  $^{161}\text{Tb}$ ) in more detail (6-10). In terms of a clinical translation,  $^{152}\text{Tb}$  was the only terbium radioisotope that was applied to patients in two independent proof-of-concept studies (11,12).  $^{152}\text{Tb}$ -DOTATOC, a somatostatin receptor (SSTR) agonist, was administered to a patient with metastatic neuroendocrine neoplasm (NEN) of the ileum, at Zentralklinik Bad Berka, Germany (11). The PET images were convincing and, owing to the relatively long half-life of  $^{152}\text{Tb}$  ( $T_{1/2} = 17.5$  h), scanning over an extended time period was feasible and enabled the visualization of the metastases (11).

$^{161}\text{Tb}$  is, nevertheless, at the most advanced stage of all Tb radioisotopes in terms of production and preclinical investigations. This radionuclide is of particular interest for targeted radionuclide therapy because of (i) its similar decay properties to those of  $^{177}\text{Lu}$  regarding the half-life ( $^{161}\text{Tb}$ :  $T_{1/2} = 6.95$  d (13) vs.  $^{177}\text{Lu}$ :  $T_{1/2} = 6.65$  d) and (ii) the emission of medium-energy  $\beta^-$ -particles ( $^{161}\text{Tb}$ :  $E\beta^- = 154$  keV vs.  $^{177}\text{Lu}$ :  $E\beta^- = 134$  keV). Importantly,  $^{161}\text{Tb}$  emits (iii) a substantial number of conversion and Auger electrons which are believed to make  $^{161}\text{Tb}$  more effective than  $^{177}\text{Lu}$  (14). Several theoretical dosimetry studies consistently predicted the high potential of this radionuclide for nuclear oncology purposes (15-20). Preclinically, it was consistently shown that  $^{161}\text{Tb}$ -labeled tumor targeting agents delayed the tumor growth in mice more effectively than their  $^{177}\text{Lu}$ -labeled counterparts (7,9,21). It was also demonstrated in preclinical studies as well as in clinical phantom studies that  $^{161}\text{Tb}$  can be visualized using SPECT due to the emission of  $\gamma$ -radiation and, thus, it can potentially be used for dosimetry purposes and monitoring the activity distribution in patients (7,9,22).

Lehenberger et al. demonstrated the concept of  $^{161}\text{Tb}$  production using the  $^{160}\text{Gd}(n,\gamma)^{161}\text{Gd} \rightarrow ^{161}\text{Tb}$  nuclear reaction in analogy to the production of no-carrier-added  $^{177}\text{Lu}$  (14). More recently, this production route was stepwise optimized at Paul Scherrer Institute, which enabled the preparation of  $^{161}\text{Tb}$  at high activity and in a quality comparable to that of commercially available  $^{177}\text{Lu}$  (3).

In the present study, it was aimed to demonstrate a first-in-human application of  $^{161}\text{Tb}$ -DOTATOC. After irradiation of Gd-targets at a high-flux reactor to obtain  $^{161}\text{Tb}$ , the ampoules were shipped to Paul Scherrer Institute, where  $^{161}\text{Tb}$  was chemically separated from its target material. The product was transported to Zentralklinik Bad Berka, where it was directly used for the radiolabeling of DOTATOC.  $^{161}\text{Tb}$ -DOTATOC was administered to two patients with NENs for whole-body planar  $\gamma$ -scintigraphy, as well as for SPECT/CT imaging.

## **MATERIALS AND METHODS**

### **Production of $^{161}\text{Tb}$**

$^{161}\text{Tb}$  was produced using the  $^{160}\text{Gd}(n,\gamma)^{161}\text{Gd} \rightarrow ^{161}\text{Tb}$  nuclear reaction, as previously reported (3,14). In brief, enriched  $^{160}\text{Gd}$  targets were irradiated at the RHF at Institut Laue Langevin in Grenoble, France, or at the SAFARI-1 reactor at Necsa, Pelindaba, South Africa.  $^{161}\text{Tb}$  was chemically separated from the Gd target material and other impurities, as previously reported (3).

### **Radiosynthesis of $^{161}\text{Tb}$ -DOTATOC for Patient Application**

The  $^{161}\text{Tb}$  product was used to radiolabel DOTATOC (JPT Peptide Technologies GmbH, Berlin, Germany) at Zentralklinik Bad Berka. In brief, a solution of DOTATOC (60  $\mu\text{g}$  and 250  $\mu\text{g}$ , respectively) in sodium acetate buffer (500  $\mu\text{L}$ , 1 M, pH = 5.5) was added to a solution of  $^{161}\text{TbCl}_3$  in 0.05 M HCl (629 – 1740 MBq; 100  $\mu\text{L}$ ). The reaction mixture was incubated at 95 °C for 30 min. Quality control was performed using analytical HPLC (Jasco PU-1580 system) equipped with a radiometric detector and a reversed-phase column (Jupiter™ Proteo, Phenomenex). The reaction solution was diluted with 5 mL sterile saline and filtered using a 0.2  $\mu\text{m}$ -sterile filter. Samples were taken for sterility and endotoxin testing using an Endosafe-PTS™ cartridge. The pH value of the final product was ~5.

### **Ethical and Regulatory Issues for Patient Application**

$^{161}\text{Tb}$ -DOTATOC was applied to the patients in compliance with the German Medicinal Products Act (Section 13, Subsection 2b) and the 1964 Declaration of Helsinki (including subsequent amendments). The study was approved by an institutional review board and the patient signed written informed consent forms prior to the investigation, which was performed in accordance with the regulations of the German Federal Agency for Radiation Protection (23). Written informed consent was obtained by the patient for collection and storage of his data in the institutional electronic data bank, and for publication of the data.

## Patient Selection and Characteristics

*Patient 1.* A 35-year-old male, suffering from a well-differentiated, non-functional malignant right glomus caroticum tumor (paraganglioma, Ki-67 5%) with lymph node, pulmonary, hepatic, and osseous metastases was selected for this study (Table 1, Supplemental Table 1). Upon diagnosis in 2011, he underwent right neck dissection, with partial excision of the primary tumor and locoregional lymphadenectomy. A session of radiochemotherapy was completed at the end of 2011. Further partial excision of the residual tumor with lymphadenectomy was performed in early 2017. From April to July 2017, the patient received two cycles of intravenously-applied peptide receptor radionuclide therapy (PRRT) using  $^{177}\text{Lu}$ -DOTATOC.  $^{68}\text{Ga}$ -DOTATOC-based PET/CT demonstrated progressive disease in July 2017, however. At the time of  $^{161}\text{Tb}$ -DOTATOC application, the patient's Karnofsky Performance Score was 90%.

*Patient 2.* A 70-year-old male suffering from metastatic, functional NEN of the pancreatic tail (G2) with lymph node and hepatic metastases was selected for the study (Table 1, Supplemental Table 1). After initial diagnosis in 1996, partial left pancreatectomy and splenectomy followed. In 2016, he was treated with everolimus which was, however, stopped due to severe stomatitis. In early 2017, the patient underwent extensive surgery for tumor debulking including right hemihepatectomy, excision of the hepatic segment 3, extirpation of lymph nodes in the hepatoduodenal ligament area and tumor excision from teres, as well as falciform ligaments, peritoneal adhesiolysis, and cholecystectomy. From 2005 to 2017, the patient received a total of nine cycles of PRRT using either an intra-arterial injection of  $^{90}\text{Y}$ -DOTATATE or an intravenous injection of  $^{177}\text{Lu}$ -DOTATATE or  $^{177}\text{Lu}$ -DOTA-LM3, a SSTR antagonist. Despite these extensive treatments, the patient experienced disease progression as demonstrated by SSTR antagonist ( $^{68}\text{Ga}$ -NODAGA-LM3)-based PET/CT. At the time of  $^{161}\text{Tb}$ -DOTATOC application, the patient's Karnofsky Performance Score was 80%.

## **SPECT/CT Imaging of $^{161}\text{Tb}$**

SPECT/CT imaging was performed using a Siemens Symbia T camera system (Siemens Healthcare GmbH, Erlangen, Germany) with the following settings: LEHR collimator, peak at 75 keV (energy window 67.1-89.5 keV, 6% upper and lower scatter window), 128x128 matrix, projections acquired with 30 s per step, step-and-shoot, body contour. The number of projections for Patient 1 and Patient 2 were 64 and 120, respectively. The following gamma camera settings were used for planar whole-body imaging: MEDISO spirit DH-V dual-headed gamma camera (Medical Imaging Systems, Budapest, Hungary), LEHR collimator, peak at 49 keV (20% energy window) and peak at 77 keV (15% energy window), scan speed 15 cm/min. SPECT images were reconstructed with a Monte-Carlo-based ordered subset expectation maximum model, using the SAREc code (22,24). The SAREc code simulates photon attenuation, scattering and the collimator-detector resolution in the forward-projection. The back-projection applied narrow beam attenuation, (without scattering). Six iterations and four subsets were used for all reconstructions.

## **Imaging of Patients after Application of $^{161}\text{Tb}$ -DOTATOC**

*Patient 1.*  $^{161}\text{Tb}$ -DOTATOC (596 MBq) was administered via a dedicated application system for radionuclide therapy into a peripheral arm vein (Table 2). Ondansetron and dexamethasone were administered intravenously as premedication to prevent possible adverse effects. An amino acid solution (consisting of 1100 mL lysine-HCl 5%, 250 mL L-arginine-HCl 10%, 250 mL NaCl 0.9%; pH value 7.4; 400 mosmol/L) was infused intravenously over a period of 4 h, along with forced diuresis using furosemide as an intravenous bolus for nephroprotection. Following the application of  $^{161}\text{Tb}$ -DOTATOC, five sets of whole-body planar (anterior and posterior) images were acquired at early timepoints (30 min and 3.0 h post injection (p.i.)), at the standard acquisition timepoint after 1 day (24 h p.i.), and at late timepoints (49.5 h and 71 h p.i.). SPECT/CT images of the thorax, as well as the abdomen and pelvis were acquired at 46 h p.i. and 46.5 h p.i., respectively.

*Patient 2.*  $^{161}\text{Tb}$ -DOTATOC (1300 MBq) was administered using the same premedication as described for Patient 1 (Table 2). As a nephroprotective measure, diuresis was forced by administration of furosemide, followed by adequate hydration with a balanced electrolyte solution (Deltajonin<sup>®</sup>, 1000 mL). After application of  $^{161}\text{Tb}$ -DOTATOC, five sets of whole-body planar (anterior and posterior) images were acquired at early timepoints (30 min and 2.5 h p.i.), at the standard acquisition timepoint after 1 day (20 h p.i.), and at late timepoints (93 h and 113 h p.i.). SPECT/CT of the liver and upper abdomen was performed at 19 h p.i..

The  $^{161}\text{Tb}$ -DOTATOC SPECT/CT images were interpreted independently by two experienced physicians (two board-certified nuclear medicine physicians, each with over ten years' experience).

### **Dosimetry Estimation**

Dosimetry was performed using planar image data of Patient 1 and Patient 2 in accordance with a previously-described protocol (25). Time-dependent activity in whole body and kidneys and, for Patient 1, also in the liver and spleen was determined by drawing regions of interest on serial whole-body scans after administration of  $^{161}\text{Tb}$ -DOTATOC. The time–activity curves of source regions were fitted to exponential functions of the first or second order to determine the time-integrated activity coefficient. The mean absorbed doses were estimated with OLINDA 2.0 software.

### **Clinical safety of $^{161}\text{Tb}$ -DOTATOC**

The patients were monitored for adverse events such as nausea, emesis, rash, erythema, pruritus, fever, etc. and potential changes in vital parameters, including blood pressure, pulse rate and temperature, immediately after the  $^{161}\text{Tb}$ -DOTATOC administration and at the follow-up review. Laboratory values, such as blood cells and relevant blood plasma parameters, were measured. The estimated glomerular filtration rate (eGFR) and the C-reactive protein (CRP), as well as relevant tumor markers were also assessed (Supplemental Table 2).

## RESULTS

### Production of $^{161}\text{Tb}$ and Preparation of $^{161}\text{Tb}$ -DOTATOC

$^{161}\text{Tb}$  was produced with product data specifications as previously defined by Gracheva et al. (3). The radiolabeling of DOTATOC with  $^{161}\text{Tb}$  was carried out for patient application at Zentralklinik Bad Berka to obtain  $^{161}\text{Tb}$ -DOTATOC at a molar activity of 6.7-9.5 GBq/ $\mu\text{mol}$ . After incubation of the reaction mixture for 30 min at 95 °C, the  $^{161}\text{Tb}$  was coordinated and no “free” (uncoordinated)  $^{161}\text{Tb}$  was detected by HPLC-based quality control. No microbial growth was detected in the final product when tested for sterility. The content of bacterial endotoxins in the final product was determined to be <10 EU/mL, in accordance with the European Pharmacopoeia (26).

### First-in-Human Application

*Physiological Biodistribution in Patient 1.* Whole-body images acquired at early timepoints demonstrated biodistribution of  $^{161}\text{Tb}$ -DOTATOC within the background soft tissue, the liver, the spleen, and both kidneys (Fig. 1A/B). Accumulation of activity in the urinary bladder was due to renal excretion of  $^{161}\text{Tb}$ -DOTATOC. At the standard image acquisition timepoint (24 h p.i.), moderate intensity of physiologically accumulated  $^{161}\text{Tb}$ -DOTATOC was observed in the liver, spleen, intestines and both kidneys, with residual activity in the bladder (Fig. 1C). Delayed images acquired 3 days after application (71 h p.i.) demonstrated that  $^{161}\text{Tb}$ -DOTATOC was continuously cleared from the normal organs and tissues (Fig. 1D). At this late timepoint, the spleen visually demonstrated comparatively high accumulation of  $^{161}\text{Tb}$ -DOTATOC (Fig. 1D). The SPECT/CT images of the thorax, abdomen and pelvis acquired 2 days after injection demonstrated physiological uptake of  $^{161}\text{Tb}$ -DOTATOC in the liver, spleen and both kidneys (Fig. 2).

*Pathological Uptake in Patient 1.* The images acquired at different timepoints following injection of  $^{161}\text{Tb}$ -DOTATOC demonstrated uptake of the radiopeptide within some of the known skeletal lesions, such as the sternum and the left frontal bone, as well as in some liver lesions. The osseous metastasis of

the sternum was evident from the 3 h p.i. images onwards and persistently visualized on delayed images up to 71 h p.i.. The whole-body planar images acquired at 24 h p.i. demonstrated distinct uptake of  $^{161}\text{Tb}$ -DOTATOC in the relatively smaller lesion in the left orbital part of the frontal bone (Fig. 1C).

Fused SPECT/CT images of the thorax (46 h p.i.) and of the abdomen/pelvis, acquired 2 days after application, demonstrated uptake of  $^{161}\text{Tb}$ -DOTATOC in the osseous sternal manubrium metastasis, as well as heterogeneously distributed uptake in the liver and spleen (Fig. 2).

*Physiological Biodistribution in Patient 2.* Early timepoint images (0.5 h and 2.5 h p.i.) following injection of  $^{161}\text{Tb}$ -DOTATOC demonstrated normal blood pool activity, including the heart and the blood vessels. Distribution of the radiopeptide was also seen in the soft tissues, liver, both kidneys, and the urinary bladder (Fig. 3A/B). Accumulation of  $^{161}\text{Tb}$ -DOTATOC was observed in kidneys on the 20 h p.i.-images and in the intestinal tract (Fig. 3C). Uptake of activity in the kidneys and in the urinary bladder was ascribed to renal excretion of  $^{161}\text{Tb}$ -DOTATOC, as is commonly also the case for  $^{177}\text{Lu}$ -DOTATOC.  $^{161}\text{Tb}$ -DOTATOC was effectively cleared from normal tissues over time, as demonstrated by the reduced activity seen on the images acquired at delayed timepoints (Fig. 3D). SPECT/CT images acquired at 19 h p.i. demonstrated physiological distribution of  $^{161}\text{Tb}$ -DOTATOC in both kidneys, as well as in normal liver tissue (Fig 4).

*Pathological Uptake in Patient 2.* The whole-body planar images obtained at multiple timepoints demonstrated accumulation of  $^{161}\text{Tb}$ -DOTATOC in the bilobar hepatic metastases as early as 0.5 h p.i., which was still seen on the images acquired at late timepoints (113 h p.i.). The multiple skeletal metastases demonstrated faint uptake of the radiopeptide at the early images at 2.5 h p.i., with further significant accumulation visible on the images acquired at 113 h after injection of  $^{161}\text{Tb}$ -DOTATOC (Fig. 3). The SPECT/CT of the liver and upper abdomen acquired at 19 h p.i. demonstrated significant accumulation of  $^{161}\text{Tb}$ -DOTATOC in the hepatic metastases, as well as moderate uptake in the multiple osseous lesions seen in the thoracolumbar spine as well as the pelvis (Fig. 4).

## Dosimetry Estimation

Dosimetry data of Patient 1 were in a similar range as expected when using  $^{177}\text{Lu}$ -DOTATOC (Supplemental Table 3). Patient 2 showed a slower renal clearance of  $^{161}\text{Tb}$ -DOTATOC and, hence, an increased absorbed kidney and whole body dose (1.5 Gy/GBq and 0.07 Gy/GBq, respectively) as compared to Patient 1 (0.8 Gy/GBq and 0.04 Gy/GBq, respectively).

## Clinical Safety of $^{161}\text{Tb}$ -DOTATOC

The administration of  $^{161}\text{Tb}$ -DOTATOC, as well as post-application imaging procedures, were well tolerated by both patients. No adverse events and no any changes in vital parameters were observed or reported by the patient during, immediately after or at follow-up review of the patient after administration of  $^{161}\text{Tb}$ -DOTATOC. According to the Common Terminology Criteria for Adverse Events (CTCAE v5.0) (27), there were no clinically significant changes in the relevant laboratory values (hematological, renal, and hepatic panel) at the subsequent follow up of the patient after administration of  $^{161}\text{Tb}$ -DOTATOC (Table 3).

## DISCUSSION

$^{161}\text{Tb}$  was suggested for clinical translation due to its favorable physical decay properties (16,18-20). Importantly,  $^{161}\text{Tb}$  can be stably coordinated with a DOTA-chelator due to its chemical similarity to  $^{177}\text{Lu}$ . It can, therefore, be applied with, potentially, any tumor-targeting agent that comprises a DOTA-chelator, as demonstrated in several preclinical studies (5,7,9,11).

The feasibility of using  $^{161}\text{Tb}$ 's emitted  $\gamma$ -radiation for clinical SPECT has recently been demonstrated with human phantoms using clinical SPECT (22). It was revealed that low-energy-high-resolution (LEHR) collimators were most suited to obtain high-resolution images and predicted that SPECT-based dosimetry for  $^{161}\text{Tb}$ -labeled radiopharmaceuticals will be feasible (22). The data presented herein are the first clinical imaging results of  $^{161}\text{Tb}$  in patients.

Two patients with SSTR-expressing malignancies received  $^{161}\text{Tb}$ -DOTATOC to analyze the distribution of the radiopeptide visualized on post-application whole-body planar and SPECT/CT imaging. The resultant images showed a similar distribution profile for  $^{161}\text{Tb}$ -DOTATOC as would be expected for  $^{177}\text{Lu}$ -DOTATOC. Considering that high inter-patient as well as high intra-patient variations of dosimetry data are expected (25), the dosimetry results of the two patients that received  $^{161}\text{Tb}$ -DOTATOC are of minor informative value. They confirmed, however, the expected tissue distribution of  $^{161}\text{Tb}$ -DOTATOC. The comparatively higher absorbed kidney and whole-body dose in Patient 2 can be ascribed to the slower kidney clearance of  $^{161}\text{Tb}$ -DOTATOC in this patient, which was due to the reduced renal function demonstrated by elevated renal plasma parameters (Supplemental Table 2) (28).

In Patient 1, despite the low administered activity of  $^{161}\text{Tb}$ -DOTATOC, the resultant images visualized previously known osseous metastases, which was in agreement with the lesions visualized on the PET/CT scan performed the previous week using  $^{68}\text{Ga}$ -DOTATOC (Fig. 5). It is not surprising that not all pathological lesions observed on  $^{68}\text{Ga}$ -DOTATOC-based PET/CT images were visualized by SPECT, which generally has lower sensitivity in comparison to the high resolution, state-of-the-art diagnostic quality of PET/CT images. In agreement with the diagnostic PET/CT image, high accumulation of  $^{161}\text{Tb}$ -DOTATOC was found in the spleen, which is a peptide-specific feature (29). Patient 2 had undergone a previous splenectomy and, consequently, accumulation of activity in the spleen was not observed in this patient and dosimetry data, therefore, not available.

The images acquired following application of  $^{161}\text{Tb}$ -DOTATOC in Patient 2 demonstrated significant radiopeptide uptake in bilobar hepatic, as well as multifocal osseous metastases with visually excellent target-to-background ratio (Fig. 4). The somewhat better image quality and detection of more pathological lesions for Patient 2 was ascribed to the fact that about twice as much activity was applied in this case. Due to multiple liver metastases in this patient, dosimetry data of the liver could not be determined.

In both patients,  $^{161}\text{Tb}$ -DOTATOC was well-tolerated without any signs of adverse events during or after the procedure, indicating that the application of  $^{161}\text{Tb}$ -DOTATOC is safe.

There is no doubt that  $^{161}\text{Tb}$  holds promise as an alternative to  $^{177}\text{Lu}$  for PRRT, however, it may be important to use a targeting agent that would fully exploit the short-ranged electron emission.

## **CONCLUSION**

The world-first patient images obtained with  $^{161}\text{Tb}$  confirmed that the emitted  $\gamma$ -radiation of  $^{161}\text{Tb}$  can be used for whole-body planar as well as SPECT/CT imaging of even low activities of injected  $^{161}\text{Tb}$ . The results of this study will serve as a basis for further investigations in patients using  $^{161}\text{Tb}$ -based radiopharmaceuticals with a step-wise escalation of the  $^{161}\text{Tb}$  activity applied, thereby, achieving therapeutic efficacy.

## **ACKNOWLEDGMENTS**

The authors thank Lebogang Sepini at Necsa for the arrangements with the shipment of irradiated targets from South Africa to Switzerland. The authors thank the people responsible for radiation safety, radioactive transport and technical assistance at Paul Scherrer Institute. Furthermore, the authors express their gratitude to the nursing staff, as well as to the nuclear medicine technologists for patient management at Zentralklinik Bad Berka.

## **Funding**

RS, NvdM, CM and RPB were awarded with the Neuroendocrine Tumor Research Foundation (NETRF) Peterson Investigator Award 2018 (U.S.A.), which was a major contribution to the funding of this project. PB and TR were supported by the Swedish Cancer Society, Swedish Radiation Safety Authority, King Gustav V. Jubilee Clinic Cancer Research Foundation, Swedish Research Council and Swedish State under the agreement between the Swedish government and the county councils, the ALF agreement.

## **Conflict of Interest**

No potential conflicts of interest relevant to this article exist.

## **Key Points**

**QUESTION:** Is it feasible to visualize metastases of patients with neuroendocrine neoplasms after injection of  $^{161}\text{Tb}$ -DOTATOC?

**PERTINENT FINDINGS:** This first-in-human application of  $^{161}\text{Tb}$  demonstrated the feasibility to image metastases of neuroendocrine neoplasms after injection of relatively low activities of  $^{161}\text{Tb}$ -DOTATOC using  $\gamma$ -scintigraphy and SPECT.

**IMPLICATIONS FOR PATIENT CARE:** The feasibility of imaging  $^{161}\text{Tb}$  in patients is an essential finding in view of  $^{161}\text{Tb}$ -based radionuclide therapy in future clinical trials.

## REFERENCES

1. Müller C, Domnanich KA, Umbricht CA, van der Meulen NP. Scandium and terbium radionuclides for radiotheranostics: current state of development towards clinical application. *Br J Radiol.* 2018;91:20180074.
2. Müller C, Zhernosekov K, Köster U, et al. A unique matched quadruplet of terbium radioisotopes for PET and SPECT and for  $\alpha$ - and  $\beta^-$ -radionuclide therapy: An in vivo proof-of-concept study with a new receptor-targeted folate derivative. *J Nucl Med.* 2012;53:1951-1959.
3. Gracheva N, Müller C, Talip Z, et al. Production and characterization of no-carrier-added  $^{161}\text{Tb}$  as an alternative to the clinically-applied  $^{177}\text{Lu}$  for radionuclide therapy. *EJNMMI Radiopharm Chem.* 2019;4:12.
4. Müller C, Fischer E, Behe M, et al. Future prospects for SPECT imaging using the radiolanthanide terbium-155 - production and preclinical evaluation in tumor-bearing mice. *Nucl Med Biol.* 2014;41 Suppl:e58-65.
5. Müller C, Vermeulen C, Johnston K, et al. Preclinical in vivo application of  $^{152}\text{Tb}$ -DOTANOC: a radiolanthanide for PET imaging. *EJNMMI Res.* 2016;6:35.
6. Müller C, Reber J, Haller S, et al. Folate receptor targeted alpha-therapy using terbium-149. *Pharmaceuticals (Basel).* 2014;7:353-365.
7. Müller C, Reber J, Haller S, et al. Direct in vitro and in vivo comparison of  $^{161}\text{Tb}$  and  $^{177}\text{Lu}$  using a tumour-targeting folate conjugate. *Eur J Nucl Med Mol Imaging.* 2014;41:476-485.
8. Müller C, Vermeulen C, Köster U, et al. Alpha-PET with terbium-149: evidence and perspectives for radiotheragnostics. *EJNMMI Radiopharm Chem.* 2017;1:5.
9. Müller C, Umbricht CA, Gracheva N, et al. Terbium-161 for PSMA-targeted radionuclide therapy of prostate cancer. *Eur J Nucl Med Mol Imaging.* 2019;accepted.
10. Umbricht CA, Köster U, Bernhardt P, et al. Alpha-PET for prostate cancer: preclinical investigation using  $^{149}\text{Tb}$ -PSMA-617. *Sci Rep.* 2019;9:17800.
11. Baum RP, Singh A, Benesova M, et al. Clinical evaluation of the radiolanthanide terbium-152: first-in-human PET/CT with  $^{152}\text{Tb}$ -DOTATOC. *Dalton Trans.* 2017;46:14638-14646.
12. Müller C, Singh A, Umbricht CA, et al. Preclinical investigations and first-in-human application of  $^{152}\text{Tb}$ -PSMA-617 for PET/CT imaging of prostate cancer. *EJNMMI Res.* 2019;9:68.
13. Duran MT, Juget F, Nadjadi Y, et al. Determination of  $^{161}\text{Tb}$  half-life by three measurement methods. *Appl Radiat Isot.* 2020;159:109085.
14. Lehenberger S, Barkhausen C, Cohrs S, et al. The low-energy beta $^-$  and electron emitter  $^{161}\text{Tb}$  as an alternative to  $^{177}\text{Lu}$  for targeted radionuclide therapy. *Nucl Med Biol.* 2011;38:917-924.

15. Bernhardt P, Benjegard SA, Kolby L, et al. Dosimetric comparison of radionuclides for therapy of somatostatin receptor-expressing tumors. *Int J Radiat Oncol Biol Phys*. 2001;51:514-524.
16. Bernhardt P, Forssell-Aronsson E, Jacobsson L, Skarnemark G. Low-energy electron emitters for targeted radiotherapy of small tumours. *Acta Oncol*. 2001;40:602-608.
17. Uusijärvi H, Bernhardt P, Rösch F, Mäcke HR, Forssell-Aronsson E. Electron- and positron-emitting radiolanthanides for therapy: aspects of dosimetry and production. *J Nucl Med*. 2006;47:807-814.
18. Hindie E, Zanotti-Fregonara P, Quinto MA, Morgat C, Champion C. Dose deposits from  $^{90}\text{Y}$ ,  $^{177}\text{Lu}$ ,  $^{111}\text{In}$ , and  $^{161}\text{Tb}$  in micrometastases of various sizes: implications for radiopharmaceutical therapy. *J Nucl Med*. 2016;57:759-764.
19. Champion C, Quinto MA, Morgat C, Zanotti-Fregonara P, Hindie E. Comparison between three promising  $\beta^-$ -emitting radionuclides,  $^{67}\text{Cu}$ ,  $^{47}\text{Sc}$  and  $^{161}\text{Tb}$ , with emphasis on doses delivered to minimal residual disease. *Theranostics*. 2016;6:1611-1618.
20. Alcocer-Avila ME, Ferreira A, Quinto MA, Morgat C, Hindie E, Champion C. Radiation doses from  $^{161}\text{Tb}$  and  $^{177}\text{Lu}$  in single tumour cells and micrometastases. *EJNMMI Phys*. 2020;7:33.
21. Haller S, Pellegrini G, Vermeulen C, et al. Contribution of Auger/conversion electrons to renal side effects after radionuclide therapy: preclinical comparison of  $^{161}\text{Tb}$ -folate and  $^{177}\text{Lu}$ -folate. *EJNMMI Res*. 2016;6:13.
22. Marin I, Ryden T, Van Essen M, et al. Establishment of a clinical SPECT/CT protocol for imaging of  $^{161}\text{Tb}$ . *EJNMMI Phys*. 2020;7:45.
23. Ministry GF. Laws and regulations of radiation protection. *The radiation protection act, Germany*. 2017:78.
24. Ryden T, Heydorn Lagerlof J, Hemmingsson J, et al. Fast GPU-based Monte Carlo code for SPECT/CT reconstructions generates improved  $^{177}\text{Lu}$  images. *EJNMMI Phys*. 2018;5:1.
25. Schuchardt C, Kulkarni HR, Prasad V, Zachert C, Müller D, Baum RP. The Bad Berka dose protocol: comparative results of dosimetry in peptide receptor radionuclide therapy using  $^{177}\text{Lu}$ -DOTATATE,  $^{177}\text{Lu}$ -DOTANOC, and  $^{177}\text{Lu}$ -DOTATOC. *Recent Results Cancer Res*. 2013;194:519-536.
26. Pharmacopeia E. Bacterial endotoxins. *European Pharmacopeia* 2019;9<sup>th</sup> edition:277-282 (german edition).
27. Services USDoHaH. Common terminology criteria for adverse events (CTCAE). 2017.
28. Svensson J, Berg G, Wangberg B, Larsson M, Forssell-Aronsson E, Bernhardt P. Renal function affects absorbed dose to the kidneys and haematological toxicity during  $^{177}\text{Lu}$ -DOTATATE treatment. *Eur J Nucl Med Mol Imaging*. 2015;42:947-955.
29. Melis M, Kaemmerer D, de Swart J, et al. Localization of radiolabeled somatostatin analogs in the spleen. *Clin Nucl Med*. 2016;41:e111-114.

**TABLE 1**

Characteristics of the Patients of this Study

<b>Characteristics</b>	<b>Patient 1</b>	<b>Patient 2</b>
Age	35 years	70 years
Gender	Male	Male
Height	183 cm	193 cm
Body weight	94 kg	85 kg
Oncologic diagnosis	Metastatic, well differentiated, non-functional malignant paraganglioma (initial presentation as right Glomus caroticum tumor)	Metastatic, functional NEN of pancreatic tail
Metastases	Lymph node, pulmonary, hepatic, osseous	Lymph node, hepatic, pulmonary, osseous, peritoneal
Proliferation rate (Ki-67)	5%	4%
Initial diagnosis	September 2011	September 1996
Genetic predisposition	c.301G>T (p.Gly101Trp) heterozygous CDKN2A	N/A
Karnofsky-index (at the time of this study)	90%	80%
Previous treatments*	Surgery (2011) Radiochemotherapy (2011) Radionuclide Therapy (2017)	Surgery (1996/2017) Chemotherapy (Everolimus; 2016) Radionuclide Therapy (2017)

NEN: neuroendocrine neoplasm; N/A: not available

\* Detailed description of previous treatments are listed in Supplemental Table 1.

**TABLE 2**Application of <sup>161</sup>Tb-DOTATOC, Premedication and Scan Times

<b>Characteristics</b>	<b>Patient 1</b>	<b>Patient 2</b>
Premedication to prevent adverse effects	Ondansetron (8 mg), i.v. Dexamethasone (8 mg), i.v.	Ondansetron (8 mg), i.v. Dexamethasone (8 mg), i.v.
Measures for nephroprotection	Furosemide (20 mg) i.v. Amino acid solution (Lys/Arg), 1600 mL i.v.	Furosemide (20 mg) i.v. Electrolyte solution, 1000 mL i.v.
Application of <sup>161</sup> Tb-DOTATOC	596 MBq, i.v. (07/2018)	1300 MBq, i.v. (11/2018)
Planar scans (whole-body)	0.5 h p.i. 3 h p.i. 24 h p.i. 49.5 h p.i. 71 h p.i.	0.5 h p.i. 2.5 h p.i. 20 h p.i. 93 h p.i. 113 h p.i.
SPECT/CT scan	22.5 h p.i. (thorax) 46 h p.i. (thorax) 46.5 h p.i. (abdomen & pelvis)	19 h p.i. (liver & abdomen)

## Figures

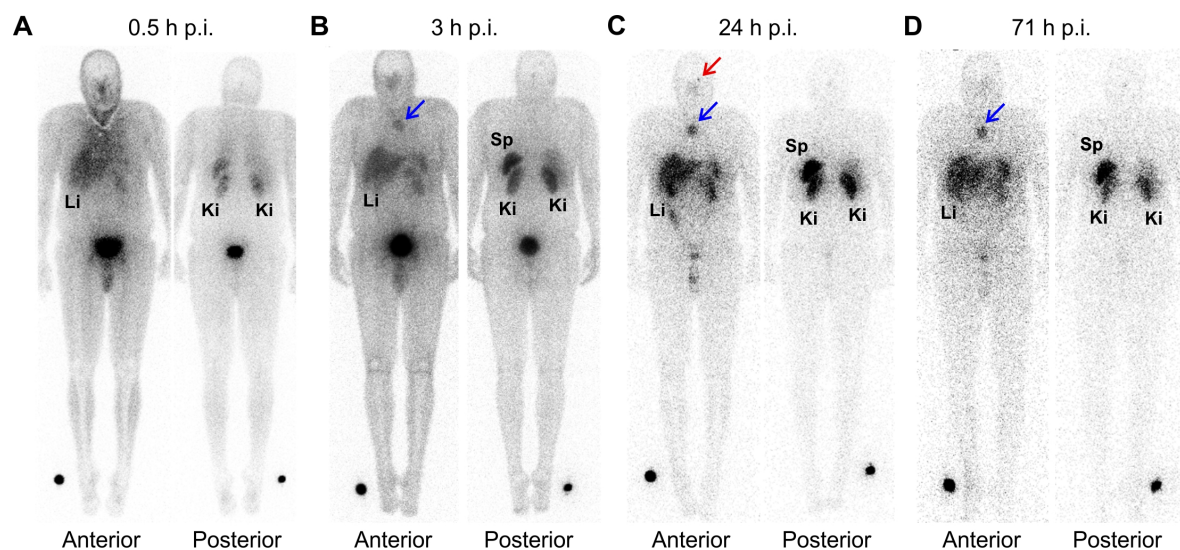


**FIGURE 1.** Whole-body images of Patient 1 obtained at 0.5 h p.i. (A), 3 h p.i. (B), 24 h p.i. (C) and 3 days (71 h) (D) after injection of  $^{161}\text{Tb}$ -DOTATOC. The images demonstrated the physiological biodistribution of  $^{161}\text{Tb}$ -DOTATOC in the liver (Li), spleen (Sp), intestines (Int), kidneys (Ki) and excretion into the urinary bladder (Bl). In addition, accumulation in the known osseous metastases (sternal manubrium, blue arrows; orbital part of the frontal bone on the left, red arrow) was visualized.

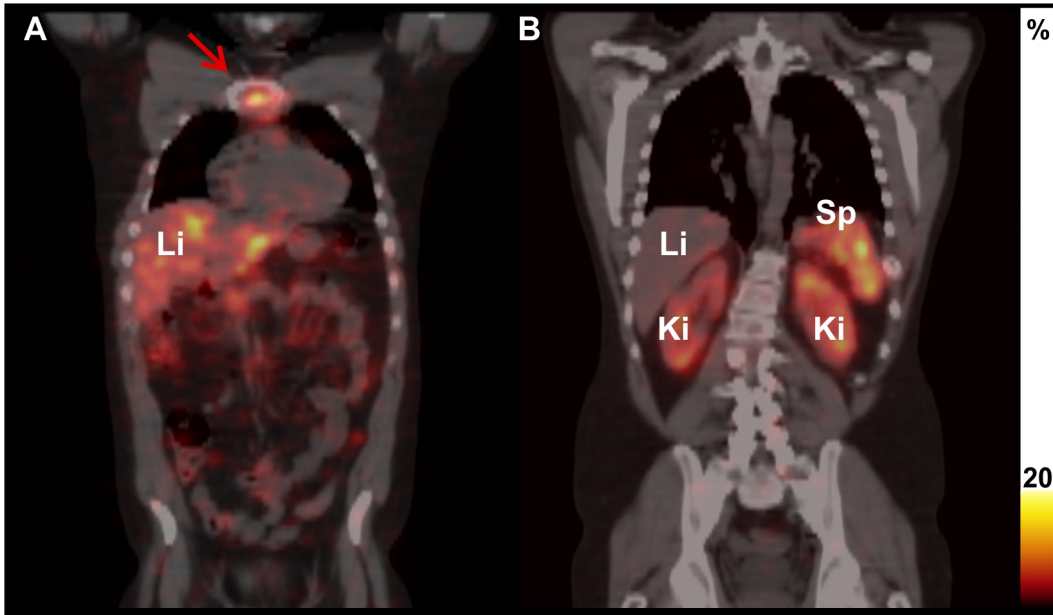


**FIGURE 2.** SPECT/CT images shown as coronal sections of Patient 1 obtained at 46 h p.i. (thorax) and 46.5 h p.i. (abdomen/pelvis) after injection of  $^{161}\text{Tb}$ -DOTATOC. The images show (A) pathological uptake of  $^{161}\text{Tb}$ -DOTATOC in an osseous metastasis (sternal manubrium, red arrow) and (B) physiological uptake of  $^{161}\text{Tb}$ -DOTATOC in the kidneys (Ki), liver (Li) and spleen (Sp).

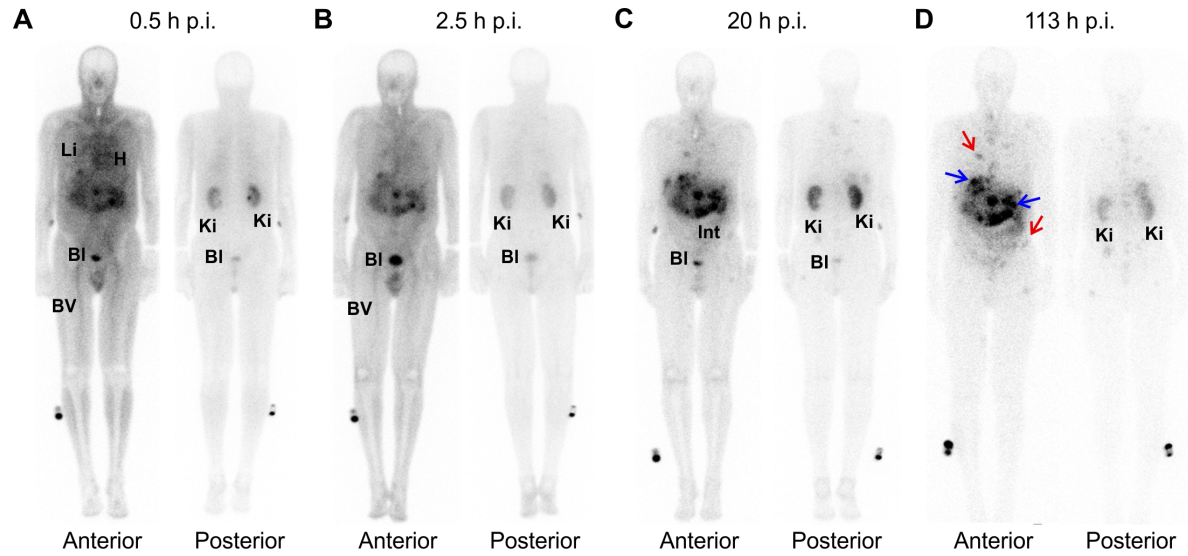


**FIGURE 3.** Whole-body images of Patient 2 obtained at 0.5 h p.i. (A), 2.5 h p.i. (B), 20 h p.i. (C) and 113 h (D) after injection of  $^{161}\text{Tb}$ -DOTATOC. Early blood-pool activity was noticed in the heart (H) and blood vessels (BV) up to 2.5 h p.i.. Physiological uptake of the radiopeptide was observed in the soft tissues, liver (Li), both kidneys (Ki), and the urinary bladder (Bl). Pathological accumulation of  $^{161}\text{Tb}$ -DOTATOC was demonstrated in bilobar liver (blue arrows) and multifocal osseous metastases (red arrows).

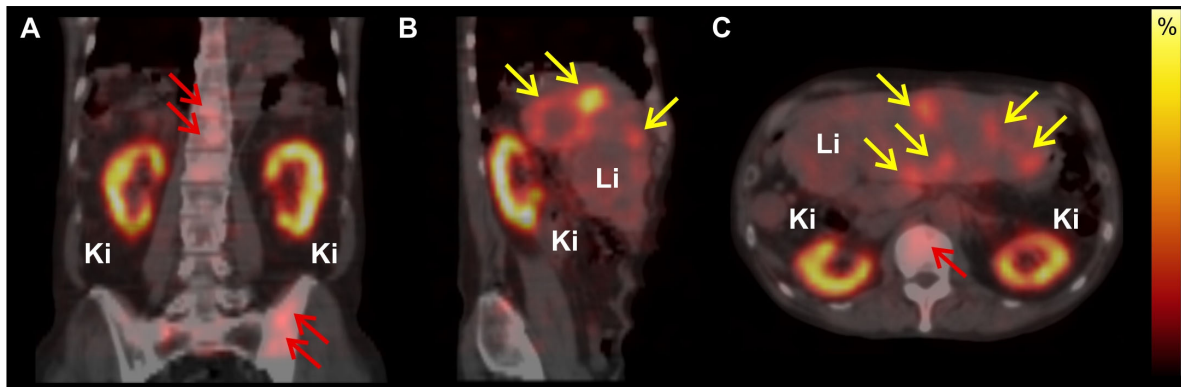


**FIGURE 4.** SPECT/CT images of Patient 2 obtained at 19 h after injection of  $^{161}\text{Tb}$ -DOTATOC. (a) Coronal section, (b) sagittal section and (c) transverse section. The images show uptake of  $^{161}\text{Tb}$ -DOTATOC in bilobar hepatic metastases (yellow arrows), as well as multiple osteoblastic skeletal metastases in the vertebral column and the pelvis (red arrows). Physiological uptake of  $^{161}\text{Tb}$ -DOTATOC is seen in both kidneys (Ki), as well as in the liver (Li).

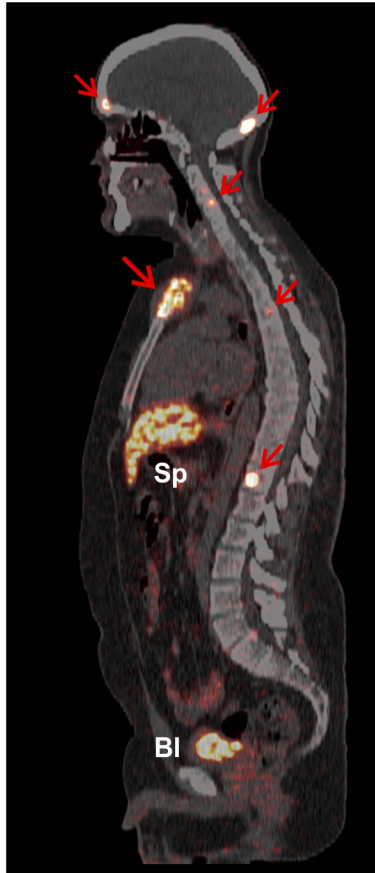


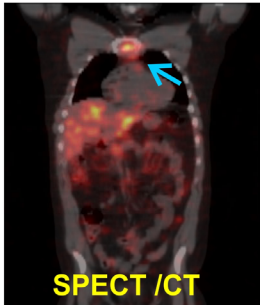
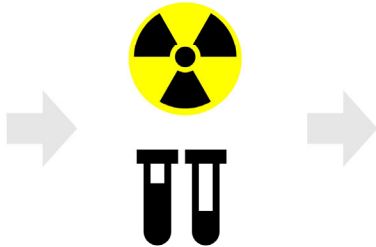
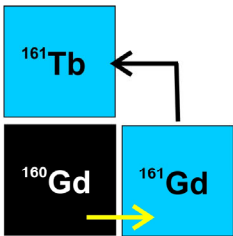
**FIGURE 5.** PET/CT sagittal section of Patient 1 obtained 60 min after injection of  $^{68}\text{Ga}$ -DOTATOC. Pathological uptake is seen in multiple skeletal metastases (sternal manubrium, left orbital part of the frontal bone, occipital bone, and in multiple vertebrae (red arrows)). Comparatively higher physiological uptake of  $^{68}\text{Ga}$ -DOTATOC was observed in the spleen (Sp). Accumulation of activity in the urinary bladder was seen due to renal excretion of the radiopeptide.

**Graphical Abstract**

Target Irradiation

Chemical Separation

Radiolabeling & Patient Application



Reactor Facilities

Research Laboratories

Radiopharmacy & Clinic

## Supplemental TABLE 1

### Previous Treatments of the Patients of this Study

Characteristics	Patient 1	Patient 2
Relevant previous surgery	09-10/2011: Embolization, followed by right neck dissection (partial excision of right glomus caroticum tumor, paraganglioma) and lymphadenectomy 01/2017: Partial excision of residual right cervical tumor and of lymph nodes	10/1996: Left partial pancreatectomy (primary tumor size 8.6 cm) and Splenectomy. 03/2017: Right hemihepatectomy, Excision of hepatic segment 3, extirpation of lymph nodes in hepatoduodenal ligament area, and tumor excision from teres as well as falciform ligaments, peritoneal adhesiolysis, cholecystectomy
Other relevant treatment	12/2011: Radiochemotherapy (59.4 Gy to the right neck, Carboplatin)	06-09/2016: Treatment with Everolimus (ceased due to severe stomatitis)
Previous PRRT	04/2017: 6800 MBq <sup>177</sup> Lu-DOTATOC i.v. 07/2017: 7100 MBq <sup>177</sup> Lu-DOTATOC i.v.	01/2005: 4600 MBq <sup>90</sup> Y-DOTATATE i.a. 05/2005: 4000 MBq <sup>90</sup> Y-DOTATATE i.a. 09/2005: 4100 MBq <sup>90</sup> Y-DOTATATE i.a. 07/2006: 7000 MBq <sup>177</sup> Lu-DOTATATE i.v. 02/2013: 7500 MBq <sup>177</sup> Lu-DOTATATE i.v. 05/2013: 8300 MBq <sup>177</sup> Lu-DOTATATE i.v. 05/2015: 5900 MBq <sup>177</sup> Lu-DOTATATE i.v. 08/2017: 6000 MBq <sup>177</sup> Lu-DOTA-LM3 i.v. 11/2017: 5800 MBq <sup>177</sup> Lu-DOTA-LM3 i.v.

NEN: neuroendocrine neoplasm; i.a.: intra-arterial; i.v.: intravenous; N/A: not available

## Supplemental TABLE 2

Laboratory Parameters of the Patients Before and After <sup>161</sup>Tb-DOTATOC Administration

Parameters	Normal range	Units	Patient 1		Patient 2	
			Before (02.07.18)	After (26.03.19)	Before (07.11.18)	After (19.12.18)
Hemoglobin	8.6–12.1	mmol/L	9.0	9.3	7.7	6.4
Leukocytes	4.3–10	Gpt/L	7.5	8.4	8.6	8.5
Thrombocytes	150–400	Gpt/L	193	166	366	377
Urea	3–9.2	mmol/L	2.6	2.3	6.2	8.9
Creatinine	62–106	μmol/L	46.5	55.6	115.3	111.6
eGFR (MDRD)	>60	mL/min/1.73m <sup>2</sup>	>60	>60	57.6	59.8
ALT	<0.83	μmol/s/L	0.61	0.73	1.02	0.55
AST	<0.85	μmol/s/L	0.48	0.53	1.13	1.29
GGT	0.17–1.19	μmol/s/L	1.17	1.16	7.98	15.18
CRP	<5	mg/L	49.6	46.4	9.7	62.6
<b>Tumor markers</b>						
NSE	<16.3	ng/mL	-	-	45.2	88.8
Chromogranin A	0–100	μg/L	-	-	523	514
Metanephrine	0–90	ng/L	33.8	<30	-	-
Normetanephrine	0–180	ng/L	99.4	123.5	-	-

“Before”: 1 day before the application of <sup>161</sup>Tb-DOTATOC; “After”: at the time of the next individually planned clinical visit for follow-up.

ALT, alanine transaminase; AST, aspartate transaminase; eGFR, estimated glomerular filtration rate; GGT: gamma-glutamyl transpeptidase; MDRD: modification of diet in renal disease; CRP: C-reactive protein; NSE: Neuron-specific enolase

### Supplemental TABLE 3

#### Dosimetry Data for $^{161}\text{Tb}$ -DOTATOC Administered to Patient 1 and Patient 2

Organ/Tissue	Effective half-life in h		Mean absorbed dose in Gy/GBq <sup>1)</sup>	
	Patient 1	Patient 2	Patient 1	Patient 2
Whole body	55	52	0.04	0.07
Kidneys	44	51	0.8	1.5
Liver	57	n.d. <sup>1)</sup>	0.1	n.d. <sup>1)</sup>
Spleen	78	n.d. <sup>2)</sup>	1.2	n.d. <sup>2)</sup>

<sup>1)</sup> The calibration reference for planar scans of Patient 1 was the whole-body scan. As Patient 2 emptied the bladder before the first scan, the simultaneously scanned vial had to be used as a reference.

<sup>2)</sup> As Patient 2 had multiple liver metastases, the mean absorbed dose to the liver could not be determined.

<sup>3)</sup> As Patient 2 underwent splenectomy, a mean absorbed dose to the spleen could not be determined.